# Potential Flowfield and Added Mass of the Idealized Hemispherical Parachute

SHUKRY K. IBRAHIM*
*FluiDyne Engineering Corporation, Minneapolis, Minn.*

**The fundamental aerodynamic problem of the steady, potential flow about the idealized parachute and the related dynamic problem of its added mass in unsteady motion are treated analytically. The parachute canopy is idealized into a rigid, nonporous, spherical shell of infinitesimal thickness and arbitrary concavity. The mathematical analysis involves an extension of the method of images to the case of two intersecting spheres forming an unsymmetrical lens and uses an old idea of Sommerfeld involving superposed spaces of three dimensions related to one another in the manner of the sheets of a Riemann surface. From the potential flow solution, an analytic expression for the velocity distribution on both concave and convex sides of the canopy is obtained, and these two velocities are related to the velocity at the corresponding point on the sphere in a very simple relation. The explicit determination of the added mass for spherical shells of arbitrary concavity obviates the current practice of making very arbitrary assumptions and opens the way to interesting studies on the dynamic stability and dynamic loading of parachutes.**

## Nomenclature

| | | |
|---|---|---|
| $A_{33}$ | = | added mass for translation in the negative $z$ direction |
| $a$ | = | radius at rim of spherical cup |
| $\tilde{a}$ | = | $a$ for $\beta \leq 3\pi/2$ |
| | = | $r_0$ for $\beta \geq 3\pi/2$ |
| $n_3$ | = | component of unit vector normal, relative to the body axes |
| $Q(\psi_0)$ | = | basic multivalued dipole at $(0, \psi_0)$ |
| $q(\psi_0)$ | = | dipole at $(0, \psi_0)$ |
| $r_0$ | = | radius of sphere |
| $S$ | = | surface area |
| $S_3$ | = | Stokes' stream function for the flow about a spherical cup with unit velocity, in the $z$ direction, at infinity |
| $s$ | = | abbreviation for $\cosh\sigma$ in the toroidal coordinate system |
| $T(\psi_0)$ | = | Stokes' stream function for the basic multivalued dipole at $(0, \psi_0)$ |
| $t(\psi_0)$ | = | Stokes' stream function for the dipole at $(0, \psi_0)$ |
| $W$ | = | path of integration |
| $(x, y, z)$ | = | Cartesian coordinates with respect to body axes |
| $(r, z, \varphi)$ | = | cylindrical coordinates |
| $(\sigma, \psi, \varphi)$ | = | toroidal coordinates |
| $(\rho, \theta)$ | = | polar coordinates |
| $\alpha$ | = | external angle at the rim of the unsymmetrical lens |
| $\beta$ | = | angle defining the concavity of the spherical cup |
| $\xi$ | = | complex quantity: $\xi = \psi + i\sigma$ |
| $\rho$ | = | mass density of the fluid |
| $\tau$ | = | abbreviation for $\cos\psi$ in the toroidal coordinate system |

***Subscripts***

| | | |
|---|---|---|
| $cv$ | = | concave |
| $cx$ | = | convex |
| $\infty$ | = | condition at infinity |

***Superscript***

| | | |
|---|---|---|
| $(n)$ | = | indicates multiplicity |

## Introduction

IN the study of dynamic stability and other problems of parachute dynamics, the inertia of the air mass induced by the motion of the canopy plays a significant role, and the added or apparent mass and the moment of inertia of the system are in most cases considerably larger than the mass and moment of inertia of the canopy alone. In fluid mechanics literature, the additional, apparent mass effect has been given various designations such as added mass, apparent mass, hydrodynamic mass, induced mass, and virtual mass. Some authors use the terms "apparent mass," "virtual mass," and "added mass" equivalently and interchangeably. In parachute work, many authors use the term "apparent mass" to designate the additional mass and the term "virtual mass" to designate the sum of body plus additional mass, but in order to avoid all possible ambiguity, we use the term "added mass" here to designate the additional apparent mass effect.

Von Karman[1] stressed the importance of the role played by added mass effects on parachute dynamics and was the first to explain the unusually large decelerations recorded when parachutes are launched at very high altitudes. He based his calculations on the added mass of a flat, circular disk, and indicated that the concavity of the parachute would tend to aggravate the effect. The explicit relations between the added mass and the concavity given here enable a quantitative determination of this effect. Von Karman also suggested an experimental method of measuring the added mass of parachutes by instantaneously releasing half the suspended weight and measuring the resulting deceleration. These suggestions were adopted by the parachute branch, Wright Air Development Center (WADC), and the results of a series of these tests were given by Heinrich.[2]

The work presented here is abstracted from an extensive theoretical investigation[3] conducted by the author in parallel with an experimental study[4] on the apparent mass and moment of inertia of parachute canopy models. Both studies were done at the University of Minnesota under the direction of H. G. Heinrich, to whom the author is grateful for initially suggesting this topic and for a long and very rewarding association in the investigation of numerous aerodynamic decelerator problems.

## Problem of the Flow about Parachute Canopies

### Idealizations and Simplifying Assumptions

The aerodynamic problem of the flow about actual parachute canopies is very complex because of their unique geometric configuration. The problem is further complicated by the flexible and porous nature of the surface, and it seems

Presented at the AIAA Aerodynamic Deceleration Systems Conference, Houston, Texas, September 7–9, 1966 (no preprint number; published in bound volume of preprints of the meeting); submitted September 16, 1966. [3.01]

* Senior Staff Engineer.

unavoidable at present, in order to proceed with any theoretical analysis, to make many simplifying assumptions. In the present investigation, the flexibility and the porosity of the parachute are both ignored and the canopies are visualized as rigid, thin-walled, umbrella-like shapes of fixed geometry. No consideration is given to viscous effects such as boundary layers or other effects triggered by viscosity, such as flow separation, wakes, and cavities.

## Potential Flowfield

### *Underlying fundamental concepts*

The mathematical derivations necessary for the present problem are rather lengthy and cannot be adequately covered in this presentation. The interested reader is referred to the original references.[3,5] The emphasis here is on the underlying physical concepts, and only the equations expressing the basic flow elements in the unfamiliar toroidal coordinates or describing the final results obtained are given without proof.

The potential flow about cup-shaped bodies representing idealized forms of parachute canopies is obtained by means of the mathematically elegant but rather difficult method of Shiffman and Spencer[5] involving the use of multifold Riemann-Sommerfeld spaces.[6] Use is made of the time-honored method of "singularities," which is based on the general principle that stream surfaces are geometrically similar to solid boundaries and that velocity potentials corresponding to the motion of objects relative to the surrounding fluid can be created by introducing suitable singularities into a field that represents the undisturbed flow pattern.

The flow past a single sphere in an unlimited field is obtained by introducing a doublet of suitable strength into a uniform flow with the axis of the doublet directed upstream. The classical procedure for obtaining the flow past two separated spheres along the axis of symmetry involves, in addition, the method of "successive images"; it is not enough to place two dipoles of suitable strength at the centers of the spheres because each dipole tends to destroy the boundary condition of the other sphere. To correct this, one introduces the images of each dipole relative to the other sphere and continues this process to obtain a convergent expression for the potential function which satisfies the boundary conditions on both spheres. Since the dipoles and their successive images lie inside the two spheres, the field external to the two spheres is free of singularities.

Starting with the mathematical viewpoint that two separated spheres have an imaginary intersection, Shiffman and Spencer[5] generalized the aforementioned procedure to the case of two intersecting spheres forming a "lenticular" object that may be symmetrical or unsymmetrical. The obvious difficulty for these cases is the presence of singularities in the fluid, and this difficulty was overcome by using "multi-

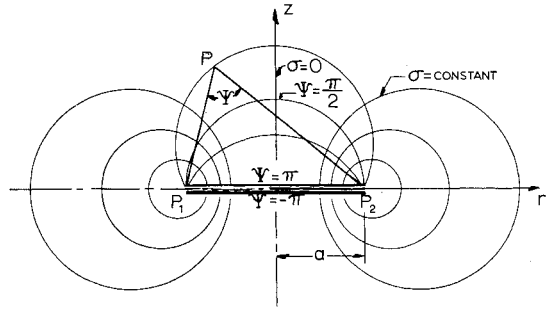


Cartesian (x,y,z): x=r cos φ; y=r sin φ; z=z

Cylindrical (r,φ,z): r = a sinh σ / (cosh σ − cos Ψ); φ = φ; z = a sin Ψ / (cosh σ − cos Ψ)

Toroidal (σ,φ,Ψ)

**Fig. 1 Toroidal coordinate system.**

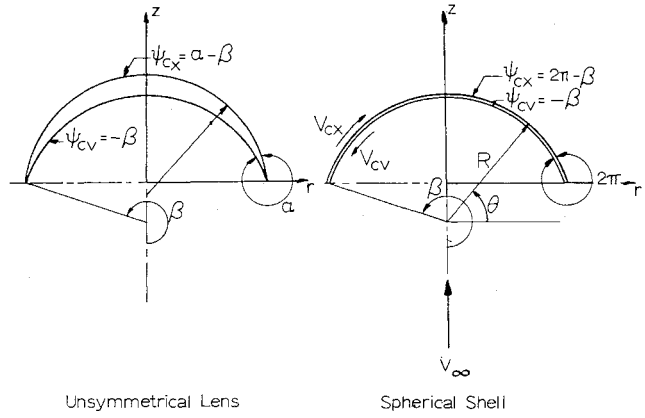


**Fig. 2 Definition sketches.**

valued" dipoles, the images of which lie in the various "sheets" of a Riemann-Sommerfeld space, and arranging that no singularities are present in that portion of the space in which we are interested.

### *Geometric considerations*

We confine our attention to unsymmetric lenses generated by two intersecting spheres and, more specifically, to spherical cups of different concavities and infinitesimal wall thickness, which may be considered as limiting cases of unsymmetric lenses generated by two intersecting spheres when the two radii and the subtended angles tend to the same values.

In dealing with spherical surfaces, a toroidal coordinate system is most appropriate. With the $z$ axis as the axis of rotation, the relations between the Cartesian $(x, y, z)$, toroidal $(\sigma, \psi, \varphi)$, and cylindrical $(r, z, \varphi)$ coordinate systems are illustrated in Fig. 1. In toroidal coordinates, surfaces with $\psi$ = constant are spherical surfaces with the circle: $r = a$, $z = 0$ as a rim or branch line, whereas surfaces with $\sigma$ = constant are ring surfaces. Because of rotational symmetry, the angle $\varphi$ will not appear in our development.

The boundary surface of an unsymmetrical lens as shown in Fig. 2 will consist of a convex and a concave spherical surface, identified by $\psi_{cx}$ and $\psi_{cv}$, respectively. In the notation adopted, an arbitrary unsymmetrical lens will be specified by: 1) $\alpha$, the external angle at the rim of the lens; 2) $\beta$, the angle specifying the concave surface as shown in Fig. 2; and 3) $a$, the radius of the rim circle. We have:

$$\psi_{cx} = \alpha - \beta \qquad \psi_{cv} = -\beta \tag{1}$$

Both $\alpha - \beta$ and $\beta$ are assumed positive and such that $\pi < \beta < 2\pi$. For the limiting case of unsymmetrical lenses of infinitesimal wall thickness, designated here as spherical shells, $\alpha \to 2\pi$ and the degree of concavity is specified uniquely by the value of $\beta$. The limiting case $\beta \to \pi$ yields the flat disk whereas $\beta \to 2\pi$ yields the sphere. The intermediate case, $\beta = 3\pi/2$, corresponds to a hemispherical shell. In order to simplify the analysis, it is assumed that the shell is moving along its axis of symmetry with unit velocity in the negative $z$ direction, in a fluid of infinite extent.

## Velocity Potential and Stream Function for Basic Flow Elements

The velocity potential for a dipole of suitable strength located at $(0, \psi_0)$ and pointing in the negative $z$ direction, in terms of toroidal coordinates, is given by

$$q(\psi_0) = \frac{a}{2}\left[\frac{(s-\tau)^{1/2}\sin(\psi-\psi_0)}{[s-\cos(\psi-\psi_0)]^{3/2}} + \frac{(s-\tau)^{1/2}\cot(\psi_0/2)}{[s-\cos(\psi-\psi_0)]^{1/2}}\right] \tag{2}$$

$$S = \frac{a^2 \sinh^2\sigma}{2(s-\tau)^{\frac{1}{2}}[s-\cos(\psi+2\beta)]^{\frac{3}{2}}} \cdot \frac{2}{\pi} \tan^{-1}\left[\left(\frac{\cosh\left(\frac{\sigma}{2}\right)+\cos\left(\frac{\psi}{2}+\beta\right)}{\cosh\left(\frac{\sigma}{2}\right)-\cos\left(\frac{\psi}{2}+\beta\right)}\right)^{\frac{1}{2}}\right]$$

$$- \frac{a^2 \sinh^2\sigma}{2(s-\tau)^2} \cdot \frac{2}{\pi} \tan^{-1}\left[\left(\frac{\cosh\left(\frac{\sigma}{2}\right)+\cos\left(\frac{\psi}{2}\right)}{\cosh\left(\frac{\sigma}{2}\right)-\cos\left(\frac{\psi}{2}\right)}\right)^{\frac{1}{2}}\right]$$

$$+ \frac{\sqrt{2}\, a^2 \sinh^2\left(\frac{\sigma}{2}\right)}{\pi(s-\tau)^{\frac{1}{2}}}\left[\frac{\cos\left(\frac{\psi}{2}+\beta\right)}{s-\cos(\psi+2\beta)} - \frac{\cos\left(\frac{\psi}{2}\right)}{s-\cos\psi}\right]$$

Where $s = \cosh\sigma$;
and $\tau = \cos\psi$

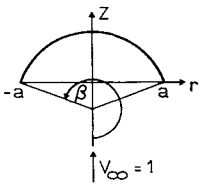


**Fig. 3 Stokes stream function for the flow past a spherical cup.**

The Stokes' stream function corresponding to $q(\psi_0)$ is given by

$$t(\psi_0) = \frac{a^2 \sinh^2\sigma}{2(s-\tau)^{1/2}[s-\cos(\psi-\psi_0)]^{3/2}} \tag{3}$$

In terms of the complex quantity, $\xi = \psi + i\sigma$. Shiffman and Spencer noted that the quantities $q(\xi)$ and $t(\xi)$ remained as potential and stream functions, were multivalued, and had branch points in the zeros of $s - \cos(\psi - \xi)$. They introduced the $n$-valued dipole and expressed its velocity potential as

$$Q^{(n)}(\psi_0) = \frac{1}{2\pi i}\int_W \frac{q(\xi)}{2n} \cot\left(\frac{\xi-\psi_0}{2n}\right) d\xi \tag{4}$$

where $W$ is a suitable path of integration in the $\xi$ plane. The potential $Q^{(n)}(\psi_0)$ is periodic in $\psi$ of period $2n\pi$.

The following two theorems[5] extend the theorem of inversion of dipoles with respect to a sphere in real space to multifold spaces and make possible the extension of the method of

$$\frac{V}{V_\infty} = \frac{\cos\theta}{\pi}\left\{3\tan^{-1}\left[\left(\frac{B^{\frac{1}{4}}+B^{-\frac{1}{4}} \mp 2\cos\left(\frac{\beta}{2}\right)}{B^{\frac{1}{4}}+B^{-\frac{1}{4}} \pm 2\cos\left(\frac{\beta}{2}\right)}\right)^{\frac{1}{2}}\right] \mp \frac{\sin\left(\frac{\beta}{2}\right)}{\sqrt{2(\cos\beta+\sin\theta)}}\left(\frac{2+3\sin\theta+\cos\beta}{1+\sin\theta}\right)\right\}$$

where $B = \frac{1-\sin(\beta-\theta)}{1+\sin(\beta+\theta)}$

The upper and lower signs relate to the Convex and Concave sides of the cup respectively

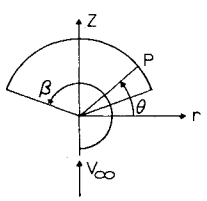


**Fig. 4 Velocity distribution on spherical cup.**

images to the construction of potential functions satisfying specified boundary conditions on spherical surfaces.

1) The function $Q(\psi_0) - Q(\psi_0')$ has a vanishing normal derivative on the spherical cap $\psi_0 = c$ if $\psi_0 + \psi_0' = 2c$ where $c$ is a constant.

2) The function $Q(\psi_0) + Q(-\psi_0)$ vanishes on $\psi = 0$. In particular $Q(0)$ vanishes on $\psi = 0$.

The Stokes' stream function conjugate to $Q^{(n)}(\psi_0)$ is

$$T^{(n)}(\psi_0) = \frac{1}{2\pi i}\int_W \frac{t(\xi)}{2n} \cot\left(\frac{\xi-\psi_0}{2n}\right) d\xi \tag{5}$$

For the special case $n = 2$ applicable to spherical cups, there is obtained

$$T^{(2)}(\psi_0) = t(\psi_0)\frac{2}{\pi} \times \tan^{-1}\left[\left(\frac{\cosh(\sigma/2)+\cos[(\psi-\psi_0)/2]}{\cosh(\sigma/2)-\cos[(\psi-\psi_0)/2]}\right)^{1/2}\right] + \frac{(2)^{1/2}\, a^2 \sinh^2(\sigma/2)\cos[(\psi-\psi_0)/2]}{\pi(s-\tau)^{1/2}[s-\cos(\psi-\psi_0)]} \tag{6}$$

The Stokes' stream function corresponding to the flow about a fixed cup with unit fluid velocity at infinity is given by

$$S_3 = T^{(2)}(-2\beta) - T^{(2)}(0) \tag{7}$$

and this yields, after suitable substitution, the expression given in Fig. 3.

### Velocity Distribution on Spherical Cups

In order to calculate the velocity distribution on both concave and convex sides of the spherical cup, it is convenient[3] to express $\sigma$ and $\psi$ in terms of polar coordinates $(\rho, \theta)$ with origin at the center of the spherical surface (Fig. 2). The nondimensional velocity distribution on any spherical cup, specified by the single parameter $\beta$, is presented in Fig. 4.

The velocity distribution on spherical cups of different concavities was calculated and compared to the velocity distribution on the sphere. The results of these calculations are illustrated in Figs. 5, 6, and 7 for a hemispherical cup ($\beta = 3\pi/2$), a shallow spherical cup ($\beta = 4\pi/3$), and a deep spherical cup ($\beta = 290°$), respectively. It is apparent from these figures that, for a certain portion of the cup, the velocity on the convex side is very nearly equal to that on the sphere whereas on the concave side it is negligibly small; this portion increases with the concavity. It is also observed that the difference between the fluid velocities on the convex and concave sides appears equal to the velocity on the surface of the sphere at the corresponding point. This result was

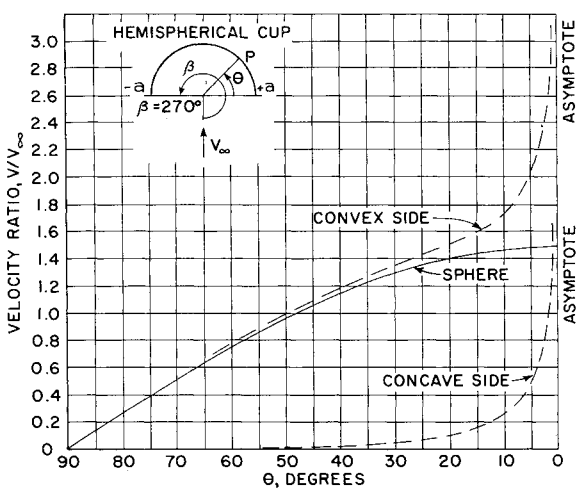


**Fig. 5 Velocity distribution on hemispherical cup.**

proved analytically.[3] As expected from potential flow theory, the velocity at the sharp edge (rim) of the cup tends to infinity.

## Added Mass for Spherical Cups

The added mass for translational motion in the negative $z$ direction may be calculated from the classical equation involving the potential function $\varphi_3$ for the motion of the cup with unit velocity in that direction:

$$A_{33} = \rho \int_S \varphi_3 n_3 \, dS \tag{8}$$

where $\rho$ represents the mass density of the fluid and $n_3$ the component of the unit vector normal relative to the $z$ direction. The calculation of the added mass by the preceding relation involves integration over the surface of the cup. A more convenient way of calculating the added mass in the present case was used[3] and yielded the following simple expression:

$$A_{33} = 2\rho a^3 \left[ \frac{2}{3} + \frac{\pi - \beta + (\frac{1}{2}) \sin 2\beta}{\sin^3 \beta} \right] \tag{9}$$

which gives the added mass for spherical cups of any concavity (specified by the angle $\beta$) in terms of the fluid density and the radius $a$ in the plane of the rim.

A special case of the spherical cup is that of the flat, circular disk ($\beta \to \pi$). Its added mass may be obtained from the preceding expression by a limiting process as follows:

$$A_{33} = 2\rho a^3 \left\{ \frac{2}{3} + \lim_{\beta \to \pi} \left[ \frac{\pi - \beta + (\sin 2\beta / 2)}{\sin^3 \beta} \right] \right\} \tag{10}$$

which yields, after repeated use of de l'Hospital's rule,

$$A_{33} = 2\rho a^3 \left[ \tfrac{2}{3} + \tfrac{2}{3} \right] = \tfrac{8}{3} \rho a^3 \tag{11}$$

This is a well-known result.

Another limiting case is that of a sphere ($\beta \to 2\pi$) with a pinhole at the bottom. (A closed sphere would violate the assumption that $\alpha = 2\pi$). For this case, one takes the limit

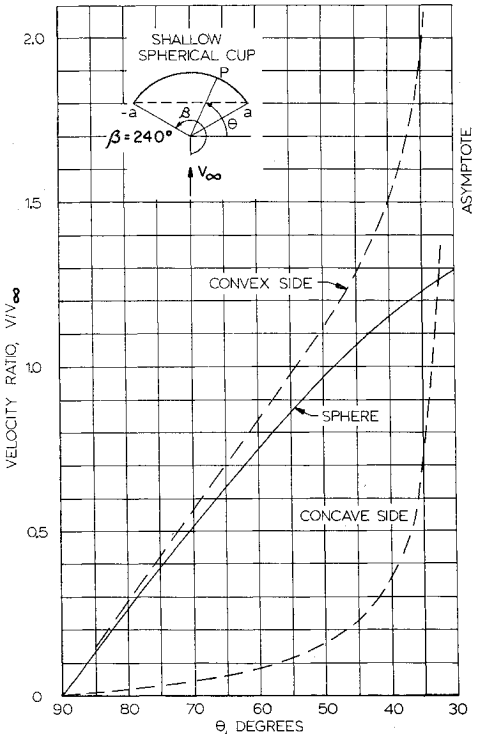


**Fig. 6 Velocity distribution on shallow spherical cup.**

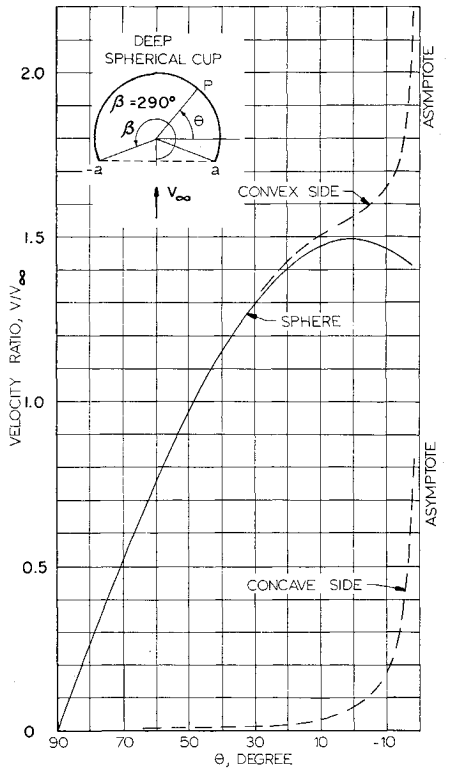


**Fig. 7 Velocity distribution on deep spherical cup.**

as $a \to 0$ and $\beta \to 2\pi$ such that

$$\lim_{\substack{a \to 0 \\ \beta \to 2\pi}} \frac{a}{\sin \beta} = -r_0 \tag{12}$$

and obtains for the added mass

$$A_{33} = 2n\rho r_0^3 \tag{13}$$

It is of interest to note that the added mass obtained for the sphere with a pinhole equals the sum of the added masses of the sphere plus the fluid mass enclosed by the spherical envelope.

The calculated values of the added mass for spherical cups of any concavity ranging between the limiting cases of the flat, circular disk and the pinholed sphere are illustrated in Fig. 8. The added masses are presented in dimensionless form by using the radius of the projected circle $\tilde{a}$ as characteristic length. The calculated values for a number of configurations are tabulated in Fig. 9, which also compares the added mass to a reference mass of a fluid sphere with $\tilde{a}$ as

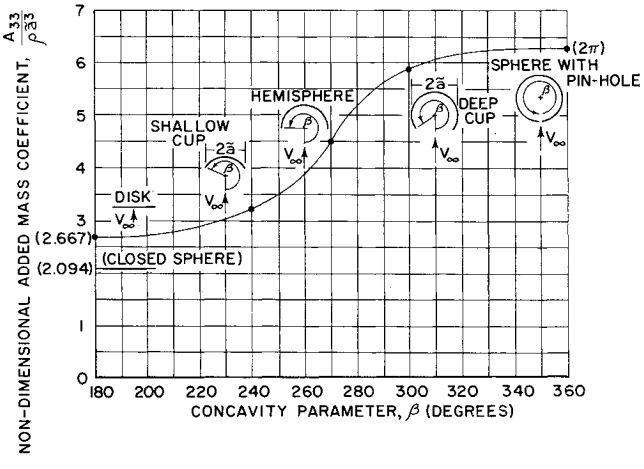


**Fig. 8 Added mass coefficients for spherical cups of different concavities.**

| $\beta$ (Degrees) | $\frac{A_{33}}{\rho \bar{a}^3}$ | $\frac{A_{33}}{M_{sph.}}$ |
|---|---|---|
| 180 | 2.667 | 0.636 |
| 182 | 2.745 | 0.655 |
| 210 | 2.783 | 0.664 |
| 240 | 3.225 | 0.770 |
| 270 | 4.475 | 1.068 |
| 300 | 5.591 | 1.334 |
| 330 | 6.269 | 1.496 |
| 355 | 6.283 | 1.499 |
| 360 | 6.2832 | 1.500 |

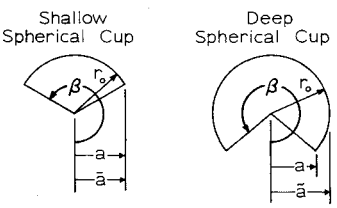


$$A_{33} = 2\rho a^3 \left( \frac{2}{3} + \frac{\pi - \beta + \frac{1}{2}\sin 2\beta}{\sin^3 \beta} \right)$$

For $\pi < \beta < \frac{3\pi}{2}$ : $\bar{a} = a = r_0 \sin\beta$ shallow spherical cup

For $\beta = \frac{3\pi}{2}$ : $\bar{a} = a = r_0$ hemispherical cup

For $\frac{3\pi}{2} < \beta < 2\pi$ : $\bar{a} = r_0 = \frac{a}{\sin\beta}$ deep spherical cup

Special limiting cases

Circular disk : $\lim_{\substack{\beta \to \pi \\ r_0 \to \infty}} r_0 \sin\beta \to -a$ : $A_{33} = \frac{8}{3}\rho a^3$

Sphere with pin-hole : $\lim_{\substack{a \to 0 \\ \beta \to 2\pi}} \frac{a}{\sin\beta} = -r_0$ : $A_{33} = 2\pi\rho r_0^3$

**Fig. 9 Added mass for spherical cups of varying concavities.**

radius. It is worth noting that the added mass is greater than the "included" fluid mass for every cup configuration.

## Concluding Comments

Through continuous development, backed up by about half a century of life-saving operational experience and supported in the last decade by extensive wind-tunnel testing, parachutes have evolved into very efficient and reliable decelerating devices. It may therefore be asked if the development of theoretical solutions of a highly idealized configuration can have more than academic interest. The answer to this question, in the author's mind, is definitely affirmative.

There is, at present, a pressing demand for an accurate analytical approach to the problems of added mass and their effects on the dynamic behavior of aerodynamic decelerators in general and parachutes in particular. This is evidenced by the rather arbitrary assumptions or the cut-and-try methods presently used to account for these effects, as, for example, the assumption of an equivalent spherical or ellipsoidal mass. Furthermore, with the continually expanding field of application of parachutes and other aerodynamic decelerators—such as the stabilization and trajectory control of bombs and torpedoes and the precision aerial delivery of cargo—and with the introduction of new and more complex configurations and the recent need for the recovery of boosters and space vehicles, including, in some cases, means of pilot trajectory control as distinct from inherent stabilization requirements, the demand for a unifying theoretical framework and a more general mode of attack of these problems will become even more acute.

The problem of the dynamic stability of parachutes is one of the important problem areas where there is a dearth of information about the added mass and moment of inertia coefficients. Earlier studies of this problem omitted consideration of the added mass effects and generally produced unrealistic results. Henn[7] appears to have been the first to take account of these effects, but, lacking more specific data, he assumed the canopy to be replaced by an air-filled ellipsoid and obtained a substantial effect of the added mass on the damping of small disturbances. Henn's equations have been extensively used since 1945. More recently, Lester[8] pointed out certain fundamental inconsistencies in Henn's analysis and mentioned that these inconsistencies had been reproduced in many current studies; they relate to an incorrect interpretation of some added mass terms in the equations. Lester stressed the importance of a more fundamental treatment of parachute dynamic stability and the need for the correct determination of the relevant added mass coefficients.

The extension of the field of application of parachutes into the supersonic regime has introduced a host of new problems including that of the heat transfer to the canopy material. The calculation of the rate of heat transfer to parachutes, particularly in the neighborhood of the stagnation point, involves the calculation of the local pressure gradient, which is readily available from the potential flow solution. It should be pointed out here that, although the general upstream flow is supersonic, the flow over the concave side of the canopy remains subsonic because of the bow shock wave. Recent tests[9] with a rigid spherical cup in supersonic flow have shown satisfactory agreement, over a substantial part of the cup on the concave side, between the measured pressure distribution and that calculated from potential flow.

The work reported here suggests many possible avenues of further investigation, such as the refinement of the analytical solution to account for canopy porosity, the calculation of the added mass in the presence of assumed cavities or wakes, and the determination of the added mass for transverse motion and of the added moment of inertia about specified axes, as well as the calculation of dynamic load distribution under unsteady conditions for the determination of shock loads and for stress analysis purposes.

## References

[1] Von Karman, T., "Note on the analysis of the opening shock of parachutes at various altitudes," Army Air Corps Scientific Advisory Group (1945).

[2] Heinrich, H. G., "Experimental parameters in parachute opening theory," Shock and Vibration Bull. 19, AD 9513, Research and Development Board, Dept. of Defense (February 1953).

[3] Ibrahim, S. K., "Apparent added mass and moment of inertia of cup-shaped bodies in unsteady incompressible flow," Univ. of Minnesota, Dept. of Aeronautics and Engineering Mechanics, Ph. D. thesis (May 1965).

[4] Ibrahim, S. K., "Experimental determination of the apparent moment of inertia of parachutes," Air Force Flight Dynamics Lab., Wright-Patterson Air Force Base, Ohio, FDL-TDR-64-153 (December 1964).

[5] Shiffman, M. and Spencer, D. C., "The flow of an ideal incompressible fluid about a lens," Quart. Appl. Mech. **V**, 270–288 (1947).

[6] Sommerfeld, A., "Uber Versweigte Potentiale im Raum," Proc. London Math. Soc. **28**, 395–429 (1897).

[7] Henn, H., "Descent characteristics of parachutes," Royal Aircraft Establishment Transl. 233 of German Report ZWB/UM/6202 (October 1944).

[8] Lester, W. G. S., "A note on the theory of parachute stability," Research and Development, British Ministry of Aviation, R & M 3352 (1962).

[9] Rose, R. E., "Experimental investigations of instability of supersonic flow about cup-shaped bodies," Univ. of Minnesota, Dept. of Aeronautics and Engineering Mechanics, Ph.D. thesis, (June 1966).